Synthesis of Size-Controlled fcc and fct FePt Nanoparticles

H. Loc Nguyen,[†] Luciano E. M. Howard,[†] Graham W. Stinton,[†] Sean R. Giblin,[†] Brian K. Tanner,[†] Ian Terry,[†] Andrew K. Hughes,[†] Ian M. Ross,[‡] Arnaud Serres,[†] and John S. O. Evans*[,†]

Department of Chemistry and Department of Physics, University Science Laboratories, University of Durham, South Road, DH1 3LE United Kingdom, and Department of Electronic and Electrical Engineering, University of Sheffield, Mappin Building, Mappin Street, Sheffield, S1 3JD United Kingdom

Received September 8, 2006. Revised Manuscript Received November 1, 2006

We report the synthesis of FePt magnetic nanoparticles using $Na_2Fe(CO)_4$ and $Pt(acac)_2$ as reagents. This method allows good control over particle stoichiometry and ensures efficient mixing of Fe and Pt atoms in the alloy at the atomic scale. The use of a variety of different high boiling solvents and different surfactants allows control over particle size. Materials can be prepared in the disordered face-centered cubic (fcc) structural form and converted to the high magnetocrystalline anisotropy face centered tetragonal (fct or $L1_0$ structure) at lower temperatures than those prepared by other routes. By using solvents such as nonadecane, docosane, and tetracosane, we can prepare samples directly in the fct form. Preformed fcc particles prepared by this method can also be transformed in solution to the fct structure. Samples have been characterized by a combination of diffraction, electron microscopy, thermogravimetric, and magnetic measurements.

Introduction

Among the many materials that have been studied for future generations of magnetic storage devices, self-assembled Ll_0 FePt nanoparticle superlattices are promising candidates because of their large uniaxial magnetocrystalline anisotropy K_u ($\sim 1 \times 10^8$ erg/cm^3) and good chemical stability.[1−4] Calculations indicate that particles as small as 2.8 nm in diameter have a sufficient high anisotropy energy K_uV (V is the magnetic grain volume) to be exploited for permanent data storage, leading to significant advances in hard disk drive areal densities over currently used materials.

There are two main requirements FePt particles must meet for this application. First, the particles must have the $L1_0$ or face-centered tetragonal (fct) structure shown in Figure 1, in which Fe and Pt atoms alternate in layers along the c direction of the tetragonal cell. This structure is responsible for the high magnetocrystalline anisotropy. This in turn requires a tight control over stoichiometry, because $L1_0$ ordering is observed only in Fe_xPt_{1-x} for $0.4 < x < 0.6$.[5,6] Second, it is necessary to control both the size and the size dispersion of the particles. Finally, for an eventual application, it is necessary to produce large mechanically stable 2D arrays of particles.

Several different routes to FePt nanoparticles have been described in the literature. The vast majority of these use solution-based methods to produce fcc particles that are subsequently transformed by thermal annealing to the high anisotropy fct phase. In their initial report, Sun et al.[1] described a polyol route to FePt that relies on the simultaneous decomposition of $Fe(CO)_5$ and reduction of $Pt(acac)_2$ in the presence of surfactants such as oleyl amine and oleic acid. Because of toxicity concerns and difficulties in controlling stoichiometry, other iron sources such as iron(III) ethoxide,[7] iron(III) acetylacetonate,[8,9] iron(II) acetate,[10] and iron(II) chloride[11] have also been investigated. Di-*n*-octyl ether has typically been the solvent of choice because of its high boiling point (297 °C), though other ether solvents such as benzyl ether[12] and phenyl ether[13] have been investigated. Polyols such as tetra-ethylene glycol (TEG)[14] and ethylene

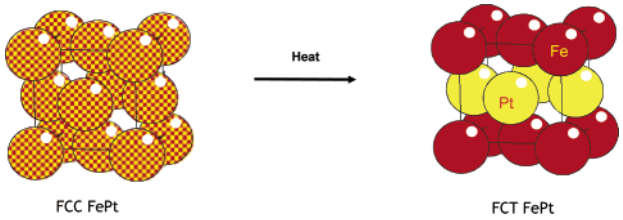

Figure 1. Schematic phase transformation of FePt nanoparticle from face-centered cubic (fcc) to face-centered tetragonal (fct) structure.

* Corresponding author. John.Evans@durham.ac.uk.
[†] University of Durham.
[‡] University of Sheffield.

(1) Sun, S. H.; Murray, C. B.; Weller, D.; Folks, L.; Moser, A. *Science* **2000**, *287*, 1989.
(2) Weller, D.; Moser, A. *IEEE Trans. Magn.* **1999**, *35* (6), 4423.
(3) Sun, S. H.; Fullerton, E. E.; Weller, D.; Murray, C. B. *IEEE Trans. Magn.* **2001**, *37* (4), 1239.
(4) Sun, S. *Adv. Mater.* **2006**, *18*, 393.
(5) Fredriksson, P. *Scand. J. Metall.* **2004**, *33*, 183.
(6) Fredriksson, P.; Sundman, B. *Calphad* **2001**, *25* (4), 535.
(7) Saita, S.; Maenosono, S. *Chem. Mater.* **2005**, *17* (26), 6624.
(8) Iwaki, T.; Kakihara, Y.; Toda, T.; Abdullah, M.; Okuyama, K. *J. Appl. Phys.* **2003**, *94* (10), 6807.
(9) Peng, D. L.; Hihara, T.; Sumiyama, K. *J. Magn. Magn. Mater.* **2004**, *277* (1−2), 201.
(10) Harpeness, R.; Gedanken, A. *J. Mater. Chem.* **2005**, *15* (6), 698.
(11) Sun, S. H.; Anders, S.; Thomson, T.; Baglin, J. E. E.; Toney, M. F.; Hamann, H. F.; Murray, C. B.; Terris, B. D. *J. Phys. Chem. B* **2003**, *107* (23), 5419.
(12) Chen, M.; Liu, J. P.; Sun, S. H. *J. Am. Chem. Soc.* **2004**, *126* (27), 8394.
(13) Wang, S.; Kang, S. S.; Nikles, D. E.; Harrell, J. W.; Wu, X. W. *J. Magn. Magn. Mater.* **2003**, *266* (1−2), 49.

10.1021/cm062127e CCC: $33.50
Published on Web 12/19/2006

Table 1. Reaction Conditions and Rietveld-Refinement-Derived Particle Sizes for fcc FePt Nanoparticles Described in This Paper

reaction	solvent	T (°C)	t (h)	surfactants (ratio used)	particle phase	particle size (nm)[a]
1	octyl ether	297	1	oleyl amine: oleic acid (1:1)	fcc	2.21(4)
2	octyl ether	297	1	oleic acid (2)	fcc	2.25(7)
3	octyl ether	297	1	oleyl amine (2)	fcc	3.28(3)
4	decyl ether	347−322	3	oleyl amine (2)	fcc	3.23(3)
5	18-crown-6	326−304	2	oleyl amine (2)	fcc	4.60(1)
6	nonadecane	334	1	oleyl amine: oleic acid (1:1)	fcc	1.67(5)
7	nonadecane	334	1	oleic acid (2)	fcc	1.73(2)
8	nonadecane	334	5	oleic acid (2)	fcc	1.83(1)
9	nonadecane	334	2	oleyl amine (2)	fct	5.07(3)
10	docosane	360	1	oleyl amine (2)	fct	6.40(9)
11	tetracosane	389−350	21	oleyl amine: oleic acid (1:1)	fcc	2.98(6)
12	tetracosane	389−382	1	oleic acid (2)	fcc	2.75(9)
13	tetracosane	389−350	21	oleyl amine (2)	fct	6.09(3)
14	tetracosane	389−370	18	oleyl amine (0.200 mL)	fct	7.75(4)

[a] Numbers in parentheses are Rietveld-derived standard uncertainties.

glycol (EG)[8,10] have recently been considered not only as reducing agents for the metallic salts but as solvents for the reaction. The majority of synthesis have used conventional heating methods, though techniques such as microwave irradiation have also been investigated.[10,15,16]

Conversion of as-synthesized fcc particles to the fct phase is normally performed thermally by heating particles to around 580 °C. This process can lead to significant particle agglomeration, leading to increases in both size and size dispersion. Different methods have been attempted to lower the FePt phase-transition temperature (T_t) and avoid particle sintering or to establish a direct route to fct nanoparticle formation. Introduction of a third metal into FePt alloys,[13,17] although reported to lower the T_t temperature, has resulted in particles shown to retain the problems of agglomeration or decomposition at high temperature. Partially ordered fct FePt nanoparticles have recently been obtained via direct synthesis on the basis of the simultaneous reduction and decomposition of iron complex and platinum salts[18,19] or co-reduction of iron and platinum salts[14,20] using conventional heating methods. However, these preliminary results have still shown a low ordering ratio and low room-temperature (RT) coercivity of fct particles, and little information relating to material characterization has been published to date. A thick SiO_2 coating was applied as a protecting shell on fcc FePt nanoparticles on the transformation into fct FePt phase without coalescence.[21] Elkins et al.[22] have also reported monodisperse fct FePt nanoparticles obtained from annealing a mixture of as-synthesized fcc FePt nanoparticles with salt powders.

To gain control over both the stoichiometry and internal structure of FePt nanoparticles, we have recently presented a straightforward, stoichiometrically controlled synthesis of FePt nanoparticles using Collman's reagent, $Na_2Fe(CO)_4$, as a reducing agent for platinum acetylacetonate, $Pt(acac)_2$.[15,23] This method has two potential advantages over other routes. First, as the reaction can be formally written as $Fe^{2-} + Pt^{2+} \rightarrow FePt$, with the electrons required to reduce Pt(II) located on the Fe source rather than on an additional species, attainment of the ideal 1:1 stoichiometry is assured. Second, the reduction step that is a key to alloy formation requires the simultaneous presence of Fe and Pt species to occur, leading to the product alloy being intimately mixed on an atomic scale. This is distinct from other methods requiring simultaneous reduction or reduction/decomposition of two metal sources, where phase separation or the formation of core−shell or locally clustered particles can take place.

In this paper, we describe the synthesis of FePt particles using this route with a variety of solvent/surfactant combinations. Different surfactant choices can be used to control the particle size produced. By using high-boiling-point solvents, we can either synthesize the magnetically important fct phase directly in solution or prepare it in solution from preformed fcc particles. Materials have been characterized by a combination of diffraction, (high resolution) transmission electron microscopy, chemical analysis, thermogravimetric analysis (TGA), magnetic measurements, and in situ high-temperature diffraction studies.

Experimental Section

General. Platinum acetylacetonate (98%) was purchased from STREM; disodium tetracarbonylferrate-dioxane complex (1:1.5), di-*n*-octyl ether (99%), 18-crown-6 (98%), oleylamine (70%), and oleic acid (90%) were obtained from Aldrich; and di-*n*-decyl ether (97%), *n*-nonadecane (99%), *n*-docosane (99%), and *n*-tetracosane (99%) were purchased from Lancaster. Ether solvents were degassed for 15 min before each use. Other AR (analytical reagents) grade organic solvents used for purification (e.g., hexane and absolute ethanol) were used as purchased. All manipulations were performed

(14) Jeyadevan, B.; Urakawa, K.; Hobo, A.; Chinnasamy, N.; Shinoda, K.; Tohji, K.; Djayaprawira, D. D. J.; Tsunoda, M.; Takahashi, M. *Jpn J. Appl. Phys. 2* **2003**, *42* (4A), L350.
(15) Nguyen, H. L.; Howard, L. E. M.; Giblin, S. R.; Tanner, B. K.; Terry, I.; Hughes, A. K.; Ross, I. M.; Serres, A.; Burckstummer, H.; Evans, J. S. O. *J. Mater. Chem.* **2005**, *15* (48), 5136.
(16) Minami, R.; Kitamoto, Y.; Chikata, T.; Kato, S. *Electrochim. Acta* **2005**, *51* (5), 864.
(17) Maeda, T.; Kai, T.; Kikitsu, A.; Nagase, T.; Akiyama, J. *Appl. Phys. Lett* **2002**, *80* (12), 2147.
(18) Kang, S. S.; Jia, Z.; Shi, S.; Nikles, D. E.; Harrell, J. W. *J. Appl. Phys.* **2005**, *97* (10), 10J318.
(19) Kang, S. S.; Jia, Z. Y.; Shi, S. F.; Nikles, D. E.; Harrell, J. W. *Appl. Phys. Lett.* **2005**, *86* (6), 62503.
(20) Sasaki, Y.; Mizuno, M.; Yu, A. C. C.; Miyauchi, T.; Hasegawa, D.; Ogawa, T.; Takahashi, M.; Jeyadevan, B.; Tohji, K.; Sato, K.; Hisano, S. *IEEE Trans. Magn.* **2005**, *41* (2), 660−664.
(21) Yamamoto, S.; Morimoto, Y.; Ono, T.; Takano, M. *Appl. Phys. Lett.* **2005**, *87* (3), 32503.
(22) Elkins, K.; Li, D.; Poudyal, N.; Nandwana, V.; Jin, Z. Q.; Chen, K. H.; Liu, J. P. *J. Phys. D* **2005**, *38* (14), 2306.
(23) Howard, L. E. M.; Nguyen, H. L.; Giblin, S. R.; Tanner, B. K.; Terry, I.; Hughes, A. K.; Evans, J. S. O. *J. Am. Chem. Soc.* **2005**, *127* (29), 10140.

under Ar using standard Schlenk line procedures unless otherwise stated. Reaction details regarding solvent, surfactant ratio, temperature, and heating time are given in Table 1.

FePt Nanoparticle Preparation in Ether Solvents. A mixture of platinum acetylacetonate (0.3 mmol) and disodium tetracarbonylferrate (0.3 mmol) were placed in a 100 mL two-necked, round-bottom flask in a N_2-filled glove box. The reaction flask was fitted to a condenser and purged with Ar before adding appropriate amounts of surfactants and solvent (10−15 mL). The reaction mixture was sonicated at 70 °C for 1 h and then heated with stirring to the boiling temperature of the solvent at a rate of 20 °C/ min. The mixture was refluxed for various time lengths to produce a dark black colloidal suspension. After reaction, the solution was cooled to room temperature (RT); the particles were precipitated by the addition of absolute ethanol (50 mL), and the mixture was sonicated for 15 min and centrifuged. After discarding the light brown supernatant, the precipitate was washed two times according to the following sequence: dispersion of particles in hexane (20 mL) with 0.05 mL of the surfactants used in the reaction, sonication at RT for 15 min, precipitation by adding ethanol (30 mL), and centrifugation to obtain the dark precipitate. The materials were dried in air at RT and subsequently stored under N_2.

FePt Nanoparticle Preparation in Hydrocarbon Solvents. A similar procedure was used for synthesis of FePt nanoparticles in hydrocarbon solvents. An appropriate amount of hydrocarbon solvent was introduced into the reaction flask either in liquid (10−15 mL for nonadecane and docosane) or solid (10 g for tetracosane) forms. The reaction mixture was sonicated at 70 °C for 1 h and then heated with stirring to the boiling point of the solvent at the rate of 20 °C/ min. The mixture was refluxed under Ar for various time periods. After the reaction, the solution was cooled to ∼40 °C before addition of hexane (30−50 mL) to dissolve the hydrocarbon solvent. A dark gel of the reaction product occasionally formed at low temperature; stirring and sonication of the mixture in hexane for 15 min were applied to break up the gel. A sufficient amount (∼5−10 mL) of absolute ethanol was added to precipitate particles but avoid crystallization of the hydrocarbon solvent. After centrifugation (1500 rpm), a black precipitate was collected, washed with hexane (40 mL) to remove remaining hydrocarbon, sonicated, and centrifuged. The dark product was repeatedly washed and recovered from a mixture of hexane (30 mL) and absolute ethanol (30 mL), and then a mixture of ethanol (40 mL) and deionized water (10 mL). The product was finally washed twice, dried, and stored according to the procedure described above.

Annealing of fcc FePt Nanoparticles in *n*-Tetracosane. A mixture of fcc FePt nanoparticles (0.150 g), oleyl amine (0.200 mL), and tetracosane (10 g) was placed in a 100 mL two-necked flask under Ar. After the tetracosane was melted (∼70 °C), the liquid mixture was sonicated at 70 °C for 1 h before heating at reflux with stirring at 389−375 °C for 18 h. After reaction, the product mixture was isolated and washed according to the method described above.

Characterization Methods. XRD data used to confirm sample structure and determine particle size were collected on a Bruker D8 Advance diffractometer equipped with a Cu tube and a Sol-X energy dispersive detector. The sample was mounted on a zero background (511) silicon wafer embedded in a generic sample holder and held in place with a thin layer of Vaseline. Data were typically collected from 10 to 90° 2θ (step size = 0.02 and time per step = 10 s) at RT. A variable divergence slit giving a constant area of sample illumination was used. XRD-derived particle sizes quoted throughout the paper were obtained from Rietveld refinements of data sets. Peak shapes were fitted by convolution of a Scherrer-type broadening term of form (λ/size)cos θ with an instrumental resolution function derived from a highly crystalline CeO_2 standard recorded under equivalent conditions. In situ variable-temperature X-ray diffraction data were collected using a Bruker AXS D8 Advance diffractometer equipped with a Cu tube, a Ge(111) incident beam monochromator (λ = 1.5406 Å) a Vantec-1 PSD, and an Anton Parr HTK1200 high-temperature furnace. Temperature calibration was determined using an external Al_2O_3/Si mixture of standards.[24−26] The powdered sample was mounted on a circular amorphous silica disk with a small amount of silicone vacuum grease as an adhesive. A slow flow of 5% H_2/95% Ar gas was passed over the sample for the experiment's duration. Fifty data sets were typically recorded over 50 h from 297 to 924K and then back to 296 K (every 25 K, 60 min each, a 0.2 K s^{-1} heating/cooling rate between temperatures, a 2θ range of 5−130°).

Information on the fcc-to-fct transition has been extracted from variable-temperature (VT) experiments by Rietveld refinement using the Topas Academic software suite. It is difficult to extract reliable quantitative information on the early stages of ordering for materials such as this, as much of the information is contained in the relatively weak, broad superlattice peaks. Because of correlations with the background (which itself has significant slowly varying contributions due to the sample mounting and furnace environment for variable temperature experiments), it is extremely hard to estimate their intensity correctly. We have therefore adopted a strategy in which the background function was fitted to each data set in an initial round of Rietveld refinements using a fully disordered model in which 2θ ranges corresponding to ordering peaks were excluded. We believe that this produces the "least-biased" estimate of the background that can be achieved at each temperature. These background polynomials were then used as fixed functions in a separate round of Rietveld refinements, in which 7 parameters (scale factor, *a* and *c* cell parameters, overall atomic displacement parameter, particle size and order parameter) were refined at each temperature. To allow refinement through the fcc → fct phase transition, a pseudo-cubic cell setting was used throughout in space group *P*4/*mmm* (Fe at 1a and 1c Wyckoff sites and Pt at 2e), and the fractional occupancy (frac) of Fe on Pt sites and Pt on Fe was allowed to refine. The order parameter for the phase transition is thus given by 1−2*frac, and ideally varies from 0 (fcc) to 1.0 (fct).

Samples for transmission electron microscopy (TEM) analysis were prepared as dilute dispersions of particles in hexane with small amounts of surfactant. A drop of particle dispersion was allowed to evaporate slowly on an amorphous carbon film supported on a standard 3 mm copper grid (200 mesh, Agar Scientific). A surfactant-exchange method[21,27] was applied for the preparation of dispersed fct FePt nanoparticles. A small amount of dry FePt nanoparticles was stirred in a mixture of absolute ethanol and tetramethylammonium hydroxide (TMAH) solution (10 wt %) for a few hours at room temperature to form a black, translucent dispersion before being depositing onto TEM grid. Preliminary TEM work was carried out on a Philips CM100 transmission electron microscope operating at 100kV. High-resolution TEM (HRTEM) was performed in a JEOL 2010F field-emission gun (FEG) microscope operating at 200 kV. Particle size distributions were obtained from TEM images and fitted using a lognormal distribution defined by $f(r) = (A/r)\exp(-(\ln(r/r_0))^2/2\sigma^2)$, with r_0 being the center radius and σ the dispersion. High spatial resolution compositional analysis was performed using an Oxford Instruments

(24) Lyon, K. G.; Swenson, C. A.; White, G. K.; Salinger, G. L. *J. Appl. Phys.* **1977**, *48*, 865.
(25) Okada, Y.; Tokumaru, Y. *J. Appl. Phys.* **1984**, *56*, 314.
(26) Taylor, D. *Br. Ceram. Trans. J* **1984**, *83*, 92.
(27) Salgueirino-Maceira, V.; Liz-Marzan, L. M.; Farle, M. *Langmuir* **2004**, *20* (16), 6946.

LINK/ISIS X-ray energy-dispersive spectrometer (EDS) (Si/Li detector, 1024 channels, 20 keV range). EDS spectra were acquired from single nanoparticles and also regions of the specimen containing clusters of particles using a 30 s preset live time acquisition. Quantification of the data was performed using the Cliff−Lorimer thin-section technique assuming an average material density of 14.6 g/cm^3 and a specimen thickness equal to the average projected diameter of the particle(s) being studied. TGA studies were carried out in Perkin-Elmer Pyris 1 TGA using Pyris version 7.0 software. All samples were mounted on uncovered platinum pans, which were heated from RT to 700 °C for solvents and surfactants and to 900 °C for FePt samples under an Ar atmosphere with a heating rate of 10 °C/min.

Magnetic measurements were carried out using a Quantum Design superconducting quantum interference device MPMS magnetometer on samples mounted in low background gelatin capsules. Magnetization as a function of applied field was measured with fields up to 50 kOe at temperatures of 10 and 290 K. Magnetization was also recorded as a function of the temperature in zero-field cooling/field cooling (ZFC/FC) experiments, where the sample was first cooled from RT to $T = 2$ K without any external field. A small field was then applied and the magnetization recorded as the temperature was increased. The FC curve was obtained by keeping the external field while the magnetization was measured as the temperature as decreased. Data are presented per gram of sample because of the difficulty in accurately assessing the percentage of surfactant/solvent molecules in an individual sample.

Results and Discussion

FePt Nanoparticles Synthesized in Ether Solvents. To compare the Fe^{2-}/Pt^{2+} synthetic route with methods previously described in the literature, we performed initial studies (reactions 1−3 of Table 1) using di-*n*-octyl ether as a solvent. Different experiments performed are summarized in Table 1. Heating $Na_2Fe(CO)_4$ and $Pt(acac)_2$ with the different surfactant combinations shown at 297 °C for 1 h led to the formation of a black suspension of FePt nanoparticles. The XRD patterns of all three recovered samples showed the chemically disordered fcc structure with broad peaks at 41, 47, 68, and 82° 2θ, which are indexed as the (111), (200), (220), and (311) peaks, respectively; the diffraction pattern of sample 1 is illustrated in Figure 2A. The fcc structure of the particles was also verified by electron diffraction, where *d*-spacings of 0.221, 0.192, 0.137, and 0.116 nm calculated from radii of pattern rings were consistent with the reflections observed by XRD. Rietveld refinement of the data performed using Topas Academic[28] suggested an average diameter of particles of 2.21(4) nm and cell parameter of 3.887(4) Å. Similar results were obtained for samples 2 and 3; particles sizes are listed in Table 1 and summarized graphically in Figure 7. A significant influence of surfactant on particle size was observed in these and related reactions. In general, oleic acid leads to the formation of smaller particles (here, 2.25(7) nm) and oleyl amine larger (3.28(3) nm). We note that use of a 1:1 acid to amine mixture gives rise to smaller particles (2.21(4) nm) than reported by Sun using the $Fe(CO)_5$/polyol synthetic route. Particles could be readily redispersed in a variety of solvents.

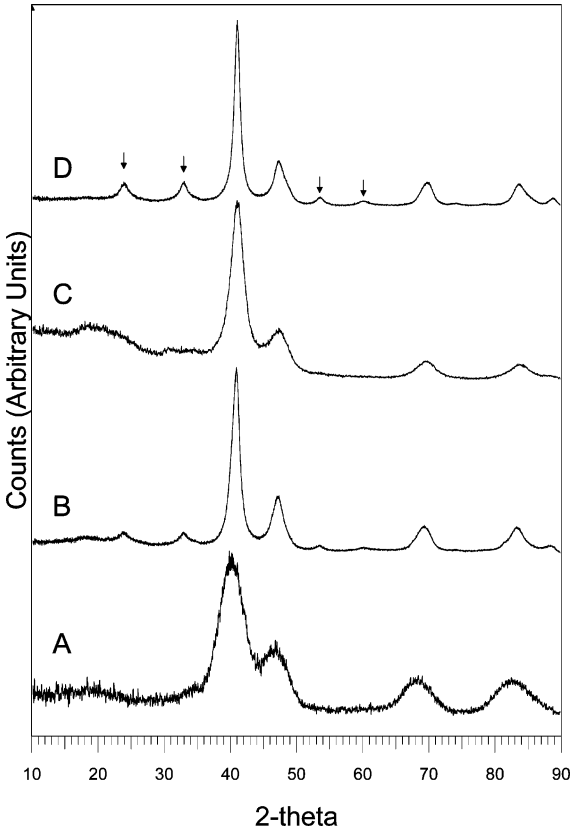

Figure 2. XRD patterns of (A) fcc FePt sample 1, (B) fct FePt sample 13, (C) fcc sample 3, and (D) fct sample 14 produced by solution annealing of sample 3. Ordering peaks discussed in the text are marked.

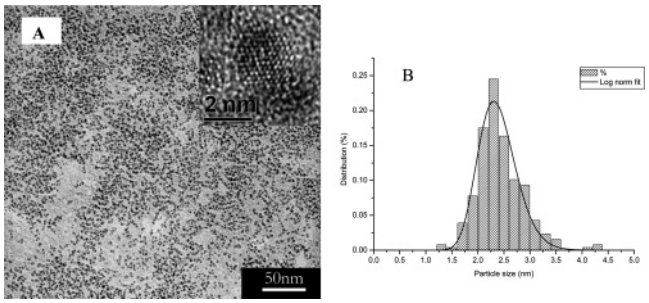

Figure 3. (A) TEM micrograph of fcc FePt particles of sample 1; insert shows a high-resolution image of an individual particle, showing it to be a single-crystalline domain with a fringe spacing consistent with the (111) planes of the fcc structure; (B) particle size distribution (average 2.36 nm, $\sigma = 0.15$, measurement of 257 particles).

Figure 3A shows a TEM micrograph of FePt particles of sample 1. These can be seen to be essentially spherical and of uniform size. Using image analysis software,[29] size measurement of 257 randomly selected particles showed a narrow size distribution. Fitting with a log-normal distribution (Figure 3B) leads to a measured mean diameter of 2.36 nm ($\sigma = 0.15$). The size is consistent with that derived from XRD measurements, suggesting that particles contain a single crystallographic domain. The HRTEM images (Figure 3A insert) of individual particles confirm particles are single crystals with lattice fringes consistent with the (111) and (200) *d*-spacing of ∼2.1 and ∼1.9 Å, respectively. EDS

(28) Coelho, A. A. *TOPAS v2.0: General Profile and Structure Analysis Software for Powder Diffraction Data*; Bruker AXS: Karlsruhe, Germany, 2000.

(29) Patel, K.; Kapoor, S.; Dave, D. P.; Mukherjee, T. *Res. Chem. Intermed.* **2006**, *32* (2), 103.

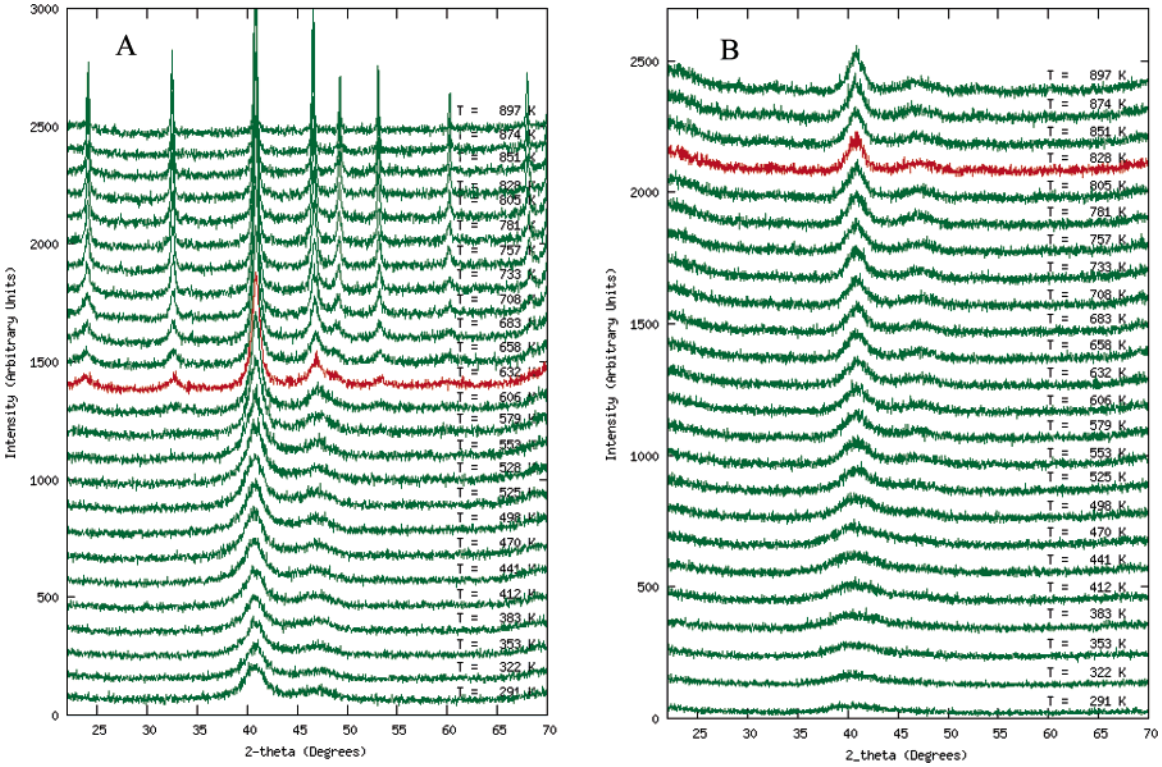

Figure 4. Twenty-five diffraction patterns of sample 3 (A) and sample 8 (B) recorded on heating as-prepared fcc FePt from ~300 to 900 K.

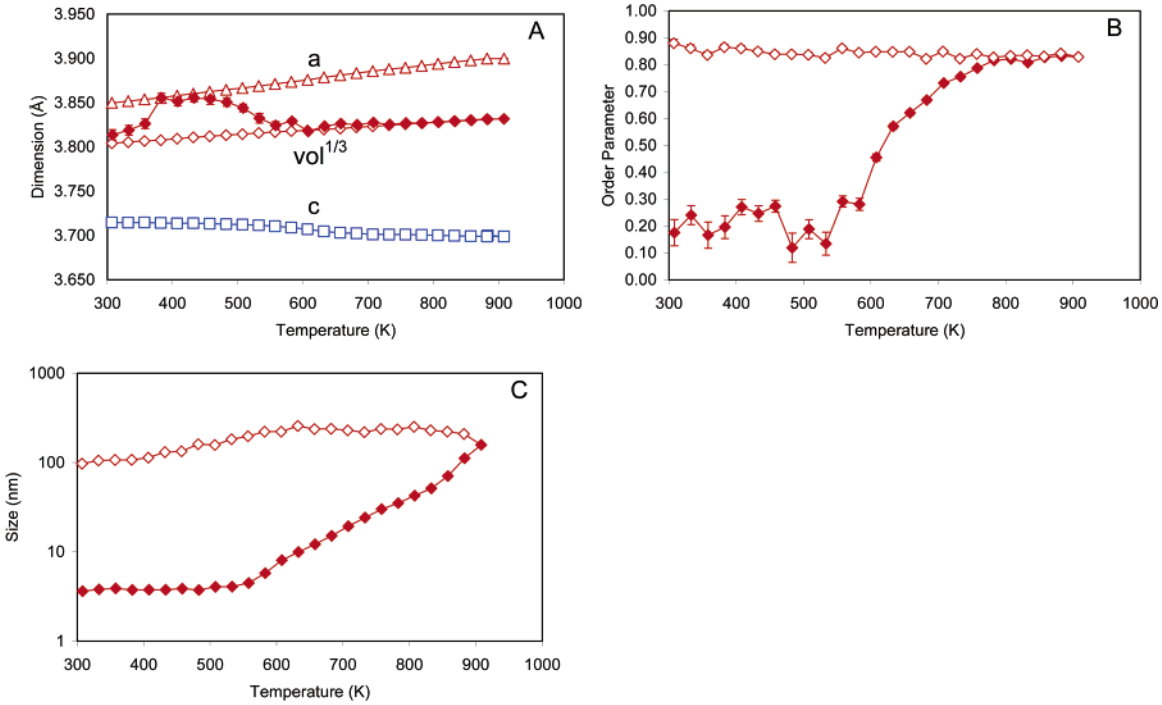

Figure 5. Rietveld refinement results for sample 1: (A) temperature dependence of the (cell volume)$^{1/3}$ on warming and cooling (closed/open diamonds, respectively) and *a* (open circles) and *c* (open squares) cell parameters on cooling; (B) order parameter on warming (closed symbols) and cooling (open symbols); (C) particle size on warming (closed symbols) and cooling (open symbols). Error bars show ±1 standard uncertainty as derived by Rietveld refinement and are probably an underestimation of the true uncertainty on parameters. Where error bars are not visible, as they are smaller than the size of the plotted symbol.

analysis of 12 clusters containing 2−6 particles each gave an overall average Fe:Pt stoichiometry of 50.2:49.8 (σ = 2.5). Analysis of individual particles revealed that a range of compositions are present with some particles either Fe or Pt rich. Yu and co-workers[30] have similarly reported that individual particles prepared by the conventional polyol synthetic route can have a wide stoichiometric range, with a significant proportion of particles being either Fe or Pt rich despite the overall bulk sample stoichiometry being close to 1:1. In fact, they report that only 29% of individual particles lie in the $0.4 < x < 0.6$ Fe_xPt_{1-x} range that would allow the

(30) Yu, A. C. C.; Mizuno, M.; Sasaki, Y.; Kondo, H. *Appl. Phys. Lett.* **2004**, *85* (25), 6242.

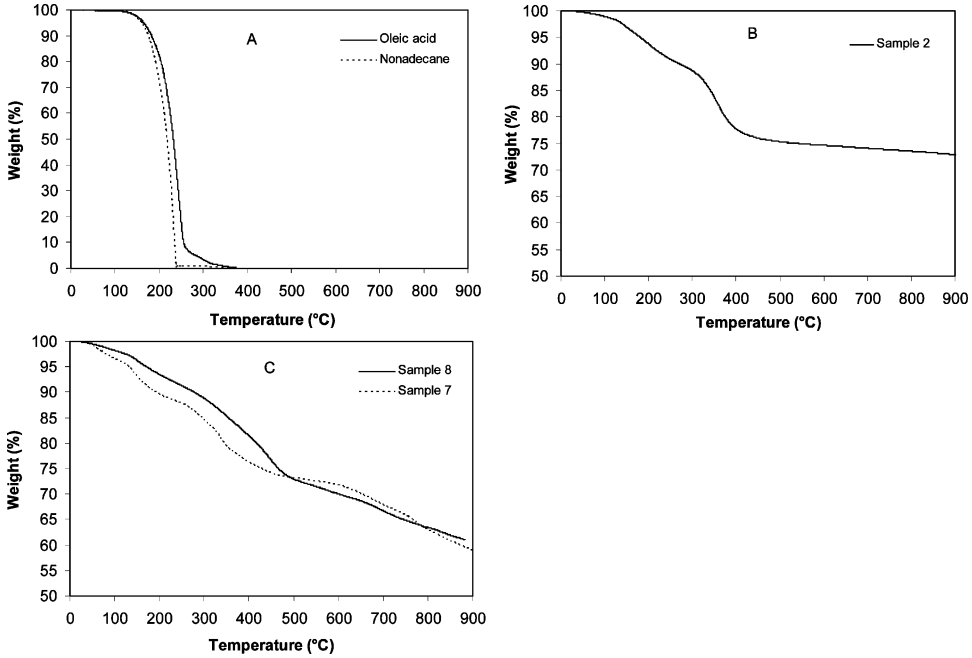

Figure 6. (A) TGA of nonadecane and oleic acid; (B) sample 2 prepared with oleic acid in octyl ether; (C) sample 7 and 8 prepared with oleic acid in nonadecane.

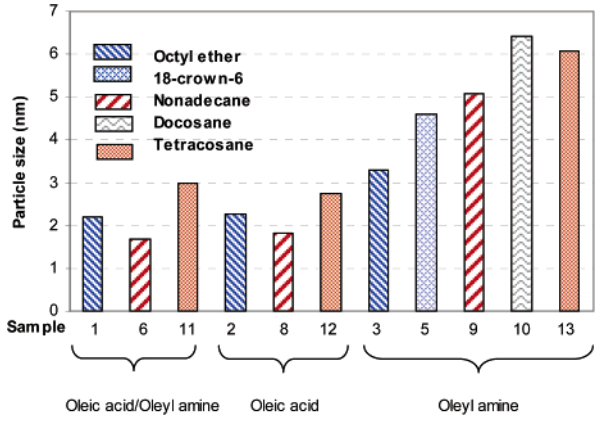

Figure 7. Variation of particle size of samples prepared with different reaction conditions.

transition to the $L1_0$ phase to occur. We note that unlike Yu et al., 83% of the individual particles prepared by this route lie within this range. This suggests that significantly better control over individual particle stoichiometry is achieved with our Fe^{2-}/Pt^{2+} synthetic route.

The fcc FePt particles prepared by this route can be converted to the magnetically important fct $L1_0$ phase by heating under a flow of 5% H_2 in Ar. Figure 4A shows a narrow 2θ range of a series of diffraction experiments of sample 3 recorded at increasing temperatures; each pattern was recorded over ~1 h with rapid heating between data collections. Two different phenomena can be observed from these data. First, from a temperature of around 632 K (359 °C), extra peaks appear at 2θ values of ~24 and 33°. These peaks can be indexed as the (001) and (110) reflections of the fct phase (using a pseudo-cubic cell of $a \approx 3.85$ Å, $c \approx 3.71$ Å) and provide direct evidence of the ordering phase transition. The recorded ordering temperature is significantly lower than the ~580 °C used to order previously reported materials. It is also clear from Figure 4A that peaks sharpen on heating, which is evidence of particle growth at higher temperatures.

Selected results extracted from Figure 4A by Rietveld refinement are shown in Figure 5. Figure 5A shows the temperature dependence of the unit,cell size. Below the fcc → fct ordering temperature, individual values of a and c are ill-defined by Rietveld refinement (the material is cubic and peaks are broad, so psuedo-cubic tetragonal values show considerable scatter), so we choose to plot (volume)$^{1/3}$ on warming, which provides an average measure of cell parameter over the whole temperature range. A significant reduction in this parameter is seen from around 450 K. A reduction in volume is expected for the fcc → fct transition and is well-known in, for example, AuCu binary alloys. We note that the reduction in cell volume occurs before significant ordering peaks are visible in Figure 4A and before significant particle growth. Cell volume is therefore perhaps the most accessible indication that particle ordering is beginning to occur. On cooling, the material retains the fct structure, as expected. Cell parameters on cooling of $a = 3.857(7)$, $c = 3.708(1)$ Å at 296 K compare to literature values of $a = 3.855$ Å, $c = 3.711$ Å,[31] or $a = 3.85$ Å, $c = 3.71$ Å.[32]A recent neutron-scattering measurement on large single crystals of bulk FePt shows a similar expansion of the c cell parameter on cooling, with a discontinuity at close to the Curie temperature of 723 K.[33]

The order parameter and particle size dependence on temperature are shown in panels B and C of Figure 5. Below ~450 K, the order parameter is approximately constant. Early in the ordering process, precise values of the order parameter

(31) Klemmer, T. J.; Shukla, N.; Liu, C.; Wu, X. W.; Svedberg, E. B.; Mryasov, O.; Chantrell, R. W.; Weller, D.; Tanase, M.; Laughlin, D. E. *Appl. Phys. Lett.* **2002**, *81* (12), 2220.
(32) *JCPDS Powder Diffraction File*; International Centre for Diffraction Data: Newtown Square, PA.
(33) Tsunoda, Y.; Kobayashi, H. *J. Magn. Magn. Mater.* **2004**, *776*, 272−276.

are hard to derive and the low-temperature values of ~0−0.2 on warming are probably not significantly different from zero; the increase in the R-factor on forcing the order parameter to be exactly 0.0 for these refinements is <0.15% for temperatures below 558 K. A significant rise in order parameter can be seen above ~550 K, a temperature slightly higher than that at which the cell volume decrease occurs. On cooling, the material retains its fct structure with the room temperature order parameter refining to 0.9, indicating a high degree of Fe/Pt ordering. The mean particle size also increases significantly from ~550 K, indicating particle sintering as the protective surfactants burn off. The minor apparent change in particle size on cooling is an instrumental artifact caused by a small movement of the sample diffracting surface from the focusing circle as the sample is cooled. Such instrumental effects are less significant for the warming data, for which the particle size contribution dominates the overall peak shape.

Similar results were also obtained for samples 1−5 of Table 1, with all samples ordering to the fct phase at 300−400 °C. These results confirm that close to stoichiometric Fe/Pt particles can be achieved by our synthetic route, which leads to samples that order to the fct phase at low temperatures.

Because VTXRD experiments on materials prepared by the Fe^{2-}/Pt^{2+} route showed that $L1_0$ ordering is possible from temperatures as low as ~330 °C, synthesis of particles was also attempted in ethers such as di-*n*-decyl ether and 18-crown-6, which are reported to have boiling points (352 and 360 °C, respectively) that would allow synthesis at temperatures above the ordering onset temperature. FePt nanoparticles (samples 4 and 5) could be successfully prepared in these solvents, and particles were isolated with sizes of 3.23(3) and 4.60(1) nm. However, despite the higher boiling points, these solvents appeared to be unstable under the reaction conditions used and reaction temperatures achievable in practice fell from ~347−322 and 326−304 °C over a 2−3 h period for di-*n*-decyl ether and 18-crown-6, respectively. In both cases, fcc materials were isolated and the temperatures of the reactions therefore appear too low to allow preparation of the fct phase.

FePt Nanoparticles Synthesized in Hydrocarbon Solvents. Because stable high (>330 °C) temperatures could not be achieved using ether solvents, reactions were also attempted in long-chain hydrocarbons such as nonadecane (bpt = 330 °C), docosane (bpt = 368 °C), or tetracosane (bpt = 391 °C). Selected reactions with various solvent/surfactant combinations are summarized in Table 1. In the presence of oleic acid as surfactant, the fcc structure was obtained for samples prepared in both nonadecane (samples 6−8) and tetracosane (samples 11 and 12). Despite high reaction temperatures (334 and 389 °C for nonadecane and tetracosane, respectively) and varied length of reaction time from 1 (sample 7) to 5 h (sample 8), powder diffraction gave no indication of the formation of fct FePt, and particles obtained were similar to those synthesized in ether solvents. However, the increase in reaction temperatures does influence the average diameters of particles, which are under 2 nm for the samples prepared in nonadecane and close to 3 nm for the samples prepared in tetracosane (samples 6, 8, and 12).

Despite the observation that reactions in nonadecane produce fcc particles similar to those obtained in ether, use of long-chain hydrocarbons may offer significant advantages in the conversion of fcc particles to fct on heating. Figure 4B shows a series of 24 X-ray diffraction patterns recorded on sample 8 prepared in nonadecane at 334 °C with oleic acid as surfactant. Upon heating, the growth of the (001) and (110) ordering peaks of the fct phase (at ~24 and ~33° 2θ) occurs from ~828 K (555 °C). The ordering temperature of sample 8 is similar to that of sample 7 and related compounds presented in our recent communication.[23] Rietveld refinement of the data shows that the order parameter rises to 0.73 for both samples 7 and 8. Crucially, the degree of particle agglomeration is significantly lower than for, e.g., sample 3, with X-ray peak widths suggesting that particles remain at smaller than 6 nm at 900 K. On cooling, the material retains the fct structure with final cell parameters of $a = 3.859(7)$ Å, $c = 3.737(8)$ Å at 296 K, in good agreement with expected values.[31−33]

The role of nonadecane in reducing particle agglomeration has been investigated by thermogravimetric analysis under Ar. Figure 6A shows the weight loss of pure nonadecane and oleic acid on heating. Both show a gradual weight loss from ~100 °C, more rapid weight loss from ~200 °C, and complete volatilization by ~250 °C. FePt sample 2, prepared using oleic acid surfactant in di-*n*-octyl ether, shows weight loss in two distinct steps between 100 and 400 °C, above which its weight remains essentially constant. We attribute this weight loss to the decomposition and evaporation of solvent and surfactant species and note that the results are broadly similar to those reported by Wu et al.[34] for a thin film of particles deposited on silicon. The results obtained for samples 7 and 8 prepared in nonadecane are markedly different (Figure 6C). Significant mass loss (~25% of total) is again observed by ~400 °C; however, the sample mass does not level off at this point but continues to fall up to the highest temperature of the experiment. It therefore appears that a nonadecane−surfactant combination provides an effective capping layer for FePt particles up to a significantly higher temperature than other solvents. This could be caused by either specific interaction between the solvent and surfactant molecules or by the formation of a carbonaceous protective coating on solvent/surfactant decomposition. Although it is possible that a portion of the continual mass loss at high temperature is due to partial reduction of surface Fe_xO_y, the effect is far more pronounced than for otherwise similar particles produced in other solvents.

In contrast to reactions with oleic acid present, carrying out the reaction in nonadecane at 334 °C with only oleyl amine as surfactant (sample 9) leads directly to the formation of a material in which fct ordering peaks are clearly visible. We emphasize that this occurs directly in solution during particle synthesis without any additional postsynthetic thermal treatment of particles. Rietveld refinement suggests an

(34) Wu, X. W.; Liu, C.; Li, L.; Jones, P.; Chantrell, R. W.; Weller, D. *J. Appl. Phys.* **2004**, *95* (11), 6810.

Table 2. Reaction Conditions and Particle Sizes of FePt Nanoparticles Synthesized with Phosphine- or Aromatic-Containing Additives

reaction	solvent	T (°C)	t (h)	surfactants (ratio used)	particle phase (order parameter)	particle size (nm)
15	doccosane	360	2	oleyl amine:TPP (2:0.5)	fct (0.40)	3.42(5)
16	docosane	360	1	oleyl amine:TOP (2:1)	fct (0.34)	3.64(5)
17	tetracosane	389−374	2	oleyl amine:C18-amine:TPP (1:2:0.5)	fct (0.42)	4.56(2)
18	tetracosane	389−370	2	oleyl amine:TPP (2:1)	fcc	2.83(5)
19	tetracosane	389−364	2	C12-aniline (1)	fct (0.39)	4.07(2)
20	tetracosane	389−364	24	C12-aniline (2)	fct (0.32)	3.84(3)

order parameter of 0.35 for the as synthesized material and a particle size of 5.07(3) nm. We note that the reaction temperature is similar to the temperature at which sample 3 (prepared at 297 °C in di-*n*-octyl ether with the same surfactant) begins to show visible ordering in the ex situ heating experiment of Figure 4A. Similar fct FePt nanoparticles were also obtained for reactions carried out in docosane (sample 10) and tetracosane (sample 13) at 360 and 389 °C, respectively; the diffraction pattern of sample 13 is shown in Figure 2B, and ordering peaks can be seen at ∼24 and ∼33° 2θ. Rietveld refinement of sample 13 gave a particle size of 6.09(3) nm and order parameter of 0.4. Recent theoretical calculations predict that fct ordering should be stable for particles above ∼2.5 nm in size but show that factors such as particle size, precise stoichiometry, and surface segregation of Fe or Pt can have a significant effect on order parameters, particularly for small particles.[35,36]

TEM micrographs (see the Supporting Information, Figure S1) of sample 13 showed a mixture of spherical particles and clumps, indicating significant agglomeration, presumably caused by the ferromagnetic properties of the particles. Selected area electron diffraction (SAED) of a cluster of small particles (see the Supporting Information, Figure S2) showed diffraction rings corresponding to *d*-spacings of ∼3.7 and ∼2.7 Å, confirming the presence of (001) and (110) ordering reflections. Chemical composition from Rutherford back scattering of bulk samples gave a 1:1 Fe:Pt stoichiometry within experimental error; EDS analysis of 40 clusters containing 1−2 grains gave an overall average Fe:Pt stoichiometry of 55.7:44.3 (σ = 0.7). Analysis of the FePt clusters revealed that a range of compositions are present, with some particles either Fe- or Pt-rich. It was found that 57.5% of the individual particles investigated lie within the $0.4 < x < 0.6$ Fe_xPt_{1-x} range that would allow the transition to the $L1_0$ phase to occur. We note that Jeyadevan[14] and Kang[19] have recently reported the formation of fct FePt nanoparticles in tetraethylene glycol and hexadecylamine at 300 and 360 °C, respectively. The reported fct FePt particle size were slightly larger (7.5 and 8 nm) than those prepared by our route. Although recent work by Jia et al.[37] indicates higher ordering by XRD patterns than earlier publications and higher room-temperature coercivity for directly synthesized fct FePt nanoparticles, the order parameters of these samples have not yet been reported.

Both a visual comparison of the intensity of ordering peaks in Figure 2B (compare to, e.g., high-temperature data of Figure 4A) and Rietveld refinement show that these particles are only partially ordered. The observation of partial order by bulk powder XRD can represent several different phenomena at the nanoparticle scale. One extreme situation is that one has a physical mixture of fully ordered and fully disordered particles present; a second extreme possibility is that all particles are chemically and structurally identical and contain partial Fe/Pt order. There are a number of other possibilities between these limits. Theoretical studies on the dependence of order parameters on precise particle stoichiometry and how they can be strongly influenced by surface segregation and local clustering, particularly for small particles, have been described recently.[35,36] The TEM observation that only around 60% of particles in this particular sample have $0.4 < x < 0.6$ suggests that this sample contains a mixture of structurally ordered and disordered particles. Some support for this observation comes from diffraction data (see the Supporting Information, Figures S3) taken on heating sample 13 from 297 to 900 K. Between 297 and 650 K, little change is observed in either diffraction data or derived order parameters. Above this temperature, the cell volume shows significant contraction and a rise in the refined order parameter is observed. On cooling back to room temperature, a refined order parameter of 0.8 and cell parameters of $a = 3.859(1)$ Å, $c = 3.731(1)$ Å are obtained, consistent with a more fully ordered phase. The observation of significant peak narrowing at these temperatures suggest that particle coalescence is required to achieve the ∼1:1 stoichiometry required for further ordering in this particular sample.

Influence of other Surfactants. The previous two sections and Table 1 show that both the particle size and internal structure of FePt nanoparticles can be straightforwardly controlled by varying synthesis temperature, solvent, and surfactants. Figure 7 attempts to summarize some of these results graphically. Several general conclusions can be drawn. In general, the use of oleic acid leads to particles smaller than using oleyl amine; syntheses with mixed surfactants lie between these two size regimes. The particle size is also directly correlated to the temperature of reaction, with syntheses in higher-boiling solvents leading to larger particle sizes. The direct synthesis of fct particles has been observed only in the absence of oleic acid and/or for larger particles. These observations are consistent with stronger acid:particle interactions than amine:particle.

It is possible to further control particle size by the addition of additional surfactant/growth inhibitor species. Table 2 summarizes a series of reactions performed in docosane/tetracosane in the presence of triphenyl phosphine (TPP), tri-*n*-octylphosphine (TOP), and 4-dodecyl aniline under conditions that lead to the formation of fct phases in their absence. Results are summarized graphically in Figure 8 alongside "control" experiments 10 and 13. The addition of phosphine/aniline-containing molecules capable of binding

(35) Chepulskii, R. V.; Butler, W. H. *Phys. Rev. B* **2005**, *72*, 134205.
(36) Müller, M.; Albe, K. *Phys. Rev. B* **2005**, *72*, 94203.
(37) Jia, Z.; Kang, S.; Shi, S.; Nikles, D. E.; Harrell, J. W. *J. Appl. Phys.* **2006**, *99*, 08E904.

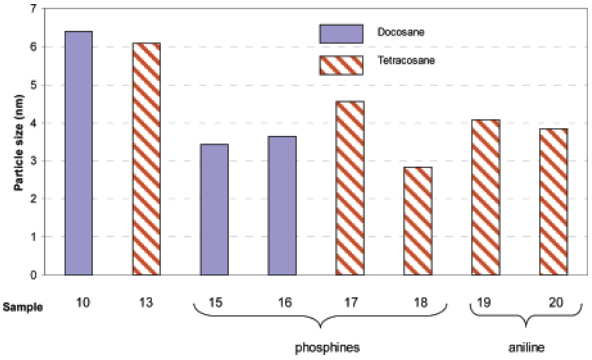

Figure 8. Comparison of particle size of samples prepared with/without phosphines and aniline as stabilizing reagents.

to growing metal surfaces leads to a significant reduction in particle size. fct ordering peaks could be observed for particles as small as 3.4 nm. We note that sample 18 (2.8 nm) shows no evidence of fct ordering. The size of particles in this sample is comparable to those prepared in the presence of oleic acid in Table 1 (maximum particle size 2.98 nm for sample 11). The experiments performed are therefore consistent with a minimum particle size for fct ordering of around 3 nm by this synthetic route. The combination of amine and aniline/phosphine surfactants provides a convenient method for tuning particle size toward this lower limit.

VTXRD studies were carried out for samples 15 and 16 and initially showed similar order parameter and particle sizes to those determined at room temperature. On heating to 300 °C and above, a gradual increase in order parameter and particle size was observed. Despite the presence of TPP and TOP, significant agglomeration of particles was observed on further heating.

fcc to fct Ordering of FePt Nanoparticles in Hydrocarbon Solvents. The observation that reactions in solvents such as nonadecane, docosane, and tetracosane can be performed at sufficiently high temperatures that fct particles can be prepared directly also offers the possibility of transforming pre-prepared fcc particles in solution. This is demonstrated by graphs C and D in Figure 2. Figure 2C shows the diffraction pattern of sample 3, an fcc material prepared in di-*n*-octyl ether at 297 °C. Figure 2D shows the diffraction pattern of the sample after heating to ~389 °C in tetracosane in the presence of oleyl amine. Clear fct ordering peaks are observed at ~24 and ~33° 2θ, and Rietveld refinement gives an order parameter of around 0.5 and a particle size of 7.75(4) nm. In our hands, samples prepared by the $Fe(CO)_5$/polyol route would not transform under these conditions. We presume this is related to the range of stoichiometries of individual particles.

These fct particles can be readily dispersed by stirring/sonicating in a mixture of ethanol and tetramethyl ammonium hydroxide. The dark suspensions so formed were typically stable for several hours before significant precipitation occurred, showing that particles are well-dispersed. Using this method of dispersal, good-quality TEM grids could be prepared. Figure 9A shows a TEM micrograph of sample 14. Image analysis (UTHSCSA Image Tool, version 3) on 1012 randomly selected clusters shows the size distribution in Figure 9B with a mean of 7.07 nm and $\sigma = 0.26$, which is consistent with the domain size obtained by XRD, again suggesting that the particles are single crystals. Selected area electron diffraction confirms that individual particles show the same ordering peaks determined by XRD. Chemical composition calculated by Rutherford back scattering of bulk samples gave a 1:1 Fe:Pt stoichiometry within experimental error, which was confirmed by EDS analysis of clusters containing ~40 particles, indicating an overall average Fe:Pt stoichiometry of 57.9:42.1. Analysis of the FePt clusters revealed that 83.3% of the individual particles investigated lie within the $0.4 < x < 0.6$ Fe_xPt_{1-x} range, which shows a high control of chemical composition of the FePt nanoparticles.

Magnetic Studies. Magnetic data are presented for selected samples from Table 1. Figure 10A shows the ZFC/FC experiment at an external applied field of 100 Oe for sample 2 prepared in octyl ether and oleic acid and shows clear evidence of superparamagnetic (SPM) behavior.[38] The low blocking temperature ($T_b = 14$ K), where the ZFC curve reaches its maximum, indicates a small particle size and the steep rise below T_b indicates a narrow size distribution, consistent with TEM results. Both the ZFC and FC curves (Figure 10B) overlap over a wide temperature range above T_b, meaning that the particles are noninteracting. This is confirmed by a plot of the inverse of magnetization as a function of temperature and its fit by a trend line that crosses the temperature axis around $T = 0$ K (inset).[39,40] Calculations and fitting of both ZFC and FC curves[41] give a rough value of the effective anisotropy $K_u \approx 2.5 \times 10^6$ ergs cm^{-3}, using an estimated particle diameter of 2.9 nm with a width of $\sigma = 0.12$. These parameters are in reasonable agreement with those values obtained from TEM measurements and XRD experiments. As expected, magnetization as a function of field (Figure 10B) taken near and above T_b ($T = 10$ and 290 K) shows practically no coercivity or remanence, whereas a hysteresis loop with a coercive field $H_C = 3.4$ kOe and a remanent magnetization $M_R = 4.02$ emu g^{-1} is observed below T_b ($T = 2$ K). This confirms the SPM behavior of the particles. Similar behavior is seen for sample 7 prepared in nonadecane with oleic acid surfactant ($T_b = 9$ K in that case).

Magnetization as a function of applied field at $T = 10$ and 290 K on sample 7 after annealing is shown in Figure 11A. Hysteresis loops are obtained with respective coercive fields $H_C = 11.1$ kOe and 2.8 kOe. Close to $H = 0$, the shape of the curve shows a sudden change in magnetization. Such a feature has already been reported in the literature and attributed to the presence of both magnetically soft and hard nanoparticles. This may occur because of the presence of both fct and fcc phases arising from either chemical composition fluctuations[42] or the particle size dependence of the fcc → fct phase transition.[23,43] Alternatively, the low field feature may be due to a single fct phase with a bimodal

(38) Neel, L. *Ann. Phys.* **1936**, *5*, 232.
(39) Chantrell, R. W.; Wohlfarth, E. P. *J. Magn. Magn. Mater.* **1983**, *40*, 1.
(40) Dormann, J. L.; Fiorani, D. *J. Magn. Magn. Mater.* **1995**, *140−144*, 451.
(41) Wohlfarth, E. P. *Phys. Lett.* **1979**, *85A*, 489.
(42) Takahashi, M.; Ogawa, T.; Hasegawa, D.; Jeyadevan, B. *J. Appl. Phys.* **2005**, *97* (10), 10J307.

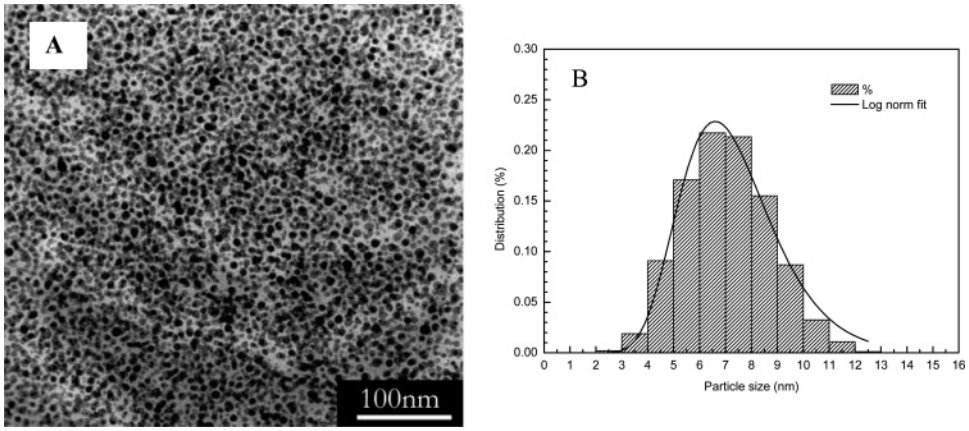

Figure 9. (A) TEM micrograph of fct FePt nanoparticles (sample 14) and (B) particle diameter histogram; the line plotted corresponds to the fit using a log-normal distribution.

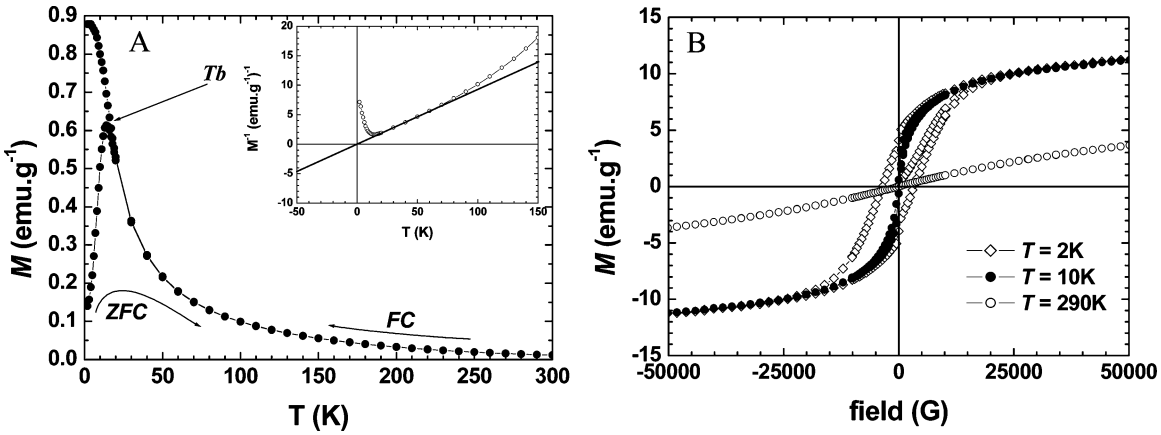

Figure 10. (A) ZFC/FC curves obtained in a field 100 Oe; inset: inverse magnetization as a function of temperature. (B) Magnetization measured as a function of field at $T = 2$, 10, and 290 K on as-prepared fcc FePt particles (sample 2).

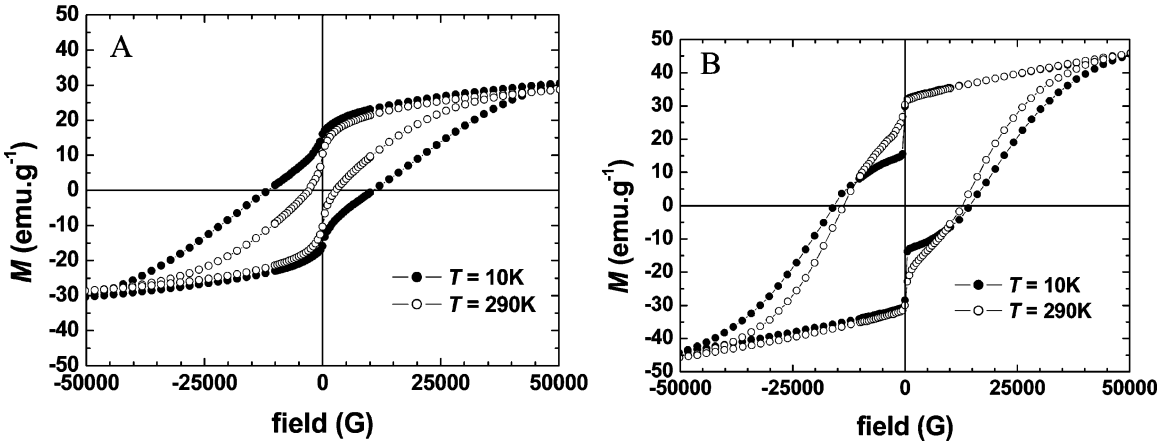

Figure 11. Hysteresis loops of postannealed FePt nanoparticles obtained on (A) sample 7, $H_C = 11.1$ kOe ($T = 10$ K) and 2.8 kOe ($T = 290$ K); (B) sample 3, $H_C = 15.1$ kOe ($T = 10$ K) and 13.2 kOe ($T = 290$ K).

switching field distribution. Our XRD data show that sample 7 has an order parameter of 0.7, so we cannot rule out the existence of both fct and fcc phases. For comparison, Figure 11b shows the M−H loop of annealed sample 3. This sample has an order parameter of 0.9 and is therefore likely to have a smaller fraction of the fcc phase than sample 7, yet it exhibits a larger low-field change in the magnetization at 10 K. In fact, the majority of the magnetization changes at low fields found in samples 3 and 7 can be attributed to particle rotation, as we have found that the low field features can be minimized by embedding the particles in solid tetracosane. We note that sample 3 exhibits coercivity of $H_C = 15.1$ kOe and 13.2 kOe at $T = 10$ and 290 K, respectively, the values being associated with the large size of the particles measured after annealing (∼110 nm).

In the case of direct synthesis of fct particles (samples 13 and 14), hysteresis loops were measured at $T = 10$ and 290 K (Figure 12). For sample 13, coercive fields of $H_C = 3.3$ and 1.3 kOe, respectively, were observed. These results show that the partially ordered FePt particles have a sufficient

(43) Ding, Y.; Majetich, S. A. *Appl. Phys. Lett.* **2005**, *87* (2), 22508.

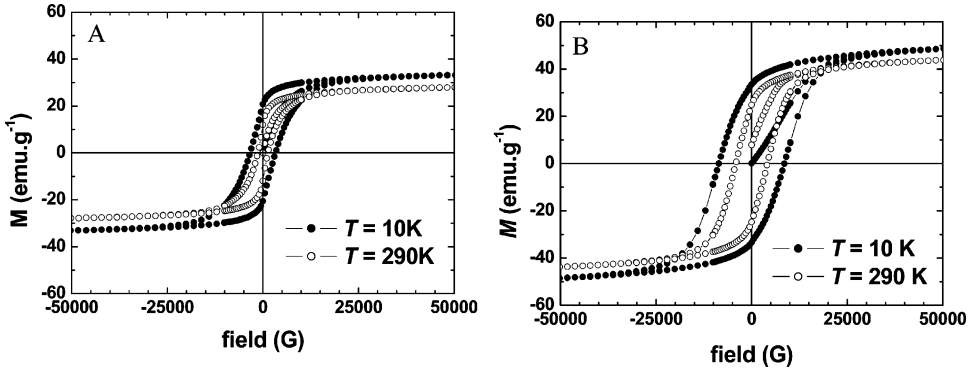

Figure 12. Magnetic hysteresis loops of fct FePt particles measured at 290 and 10 K: (A) sample 13 and (B) sample 14.

anisotropy to be ferromagnetic at room temperature. Magnetic data of sample 14 (fct FePt nanoparticles produced from fcc by heating in tetracosane solution measured as a frozen suspension in tetracosane to prevent particle realignment) show the same general tendency. Coercive fields are 8.5 and 4.1 kOe at 10 and 290 K, respectively, correlating to the larger particle size and higher fct ratio defined by XRD.

Conclusion

In conclusion, the general synthetic method presented here provides a straightforward, stoichiometrically controlled route to FePt nanoparticles. Monodispersed, superparamagnetic fcc FePt nanoparticles prepared by this route can be converted to the fct ordered FePt structure at temperatures as low as 350 °C, significantly lower than temperatures typically used for samples prepared by other routes. Using solvents such as nonadecane and tetracosane, it is possible to produce fct FePt nanoparticles directly in solution. By varying the surfactants, solvent, and temperature, the size and structural properties of FePt particles can be controlled. We believe that this synthetic method can be readily extended to the preparation of a number of metal alloys of controlled size, stoichiometry, and physical properties.

Acknowledgment. The authors thank Dr. Richard Thompson for RBS measurements, Vivian Thompson for assistance with TEM images, Douglas W. Carswell for TGA measurements, and ONE-NE (via the Durham Nanotechnology Innovation Centre) and Seagate Technology for financial support.

Supporting Information Available: Figure S1−S4: SAED pattern, TEM micrograph, Rietveld refinement data for sample 13, and larger view of Figure 9A. This material is available free of charge via the Internet at http://pubs.acs.org.

CM062127E